Article

Unified Design Principles of Inductive Power Transfer Systems for Multi-Load Applications

Jiantao Zhang [ID], **Ying Liu** * [ID]**, Chunbo Zhu and Ching Chuen Chan**

School of Electrical Engineering & Automation, Harbin Institute of Technology, Harbin 150001, China; jiantaoz@hit.edu.cn (J.Z.); zhuchunbo@hit.edu.cn (C.Z.); ccchan@eee.hku.hk (C.C.C.)
* Correspondence: cathy-ying.liu@connect.polyu.hk

Abstract: In the design of inductive power transfer (IPT) systems for multi-load applications, the versatility of the coupling structure and the choice of parameter values are crucial due to the diversity of load appliance types and operating conditions. In this paper, based on the features of various coupling structures, the equivalent circuit models of four topologies, namely single-input single-output (SISO), single-input multiple-output (SIMO), multiple-input single-output (MISO) and multiple-input multiple-output (MIMO), are established, from which general transfer characteristics are obtained and analyzed. Based on the series–series (S/S) compensation topology, a set of design principles for IPT circuits satisfying various output requirements in a multi-load environment is presented. Moreover, a control strategy to address the impedance matching issue and to facilitate communication between the primary and secondary sides is proposed. The proposed control strategy is experimentally validated.

Keywords: parameter design; multi-load; inductive power transfer; magnetic coupling

1. Introduction

With the diversifying consumers' needs and specifications of applications, electronic appliances are supporting a variety of power supply standards. The messy wires and sockets are unsightly and greatly reduce the convenience of use. Moreover, the prolonged use of wires will inevitably cause wear and tear. The aging phenomenon is extremely prone to accidents, posing safety concerns. Inductive power transfer (IPT) technology enables various appliances to be intelligent and wireless, eliminating the use of wires and reducing the risk of electric shocks [1,2]. In an IPT system, the coupling structure design can be divided into two types in terms of winding styles: One is unipolar coil [3], and the other is bipolar coil [4,5], which are both widely used, especially in the application of wireless charging for electric vehicles (EVs).According to different requirements in practical applications, coupling structures can be broadly classified into four types: single-input single-output (SISO), single-input multiple-output (SIMO), multiple-input single-output (MISO) and multiple-input multiple-output (MIMO) [6,7]. Compared with the application of wireless charging for EVs where the SISO configuration is usually adopted, the single-input double-output (SIDO) and single-input multiple-output (SIMO) configurations are mainly used in lower power applications, including consumer electronics and household appliances. For example, in public areas, compared with the mode of one cell phone matching one IPT charger, a bigger charging plane is more convenient to realize multi-load charging simultaneously. In the household appliance scenario, Wireless Power Consortium has encouraged multi-load operating application since 2013 [8]. The IPT plane helps to save area and avoid the risk of electric shock. The MIMO configuration is also adopted in the above applications to eliminate the impact of position misalignments. The research for multi-load applications has mainly focused on two aspects. The first one is the power distribution and efficiency optimization among the loads, and the other one is the

decoupling control, i.e., eliminating mutual interference among multiple loads so that each load is supported by stable power [9,10]. Mi et al. [11] have proposed a bipolar coupling structure that can provide power to multiple loads axially. The receiving (secondary) coil and the relay coil are connected in parallel, with the wires wound in a relatively orthogonal position to ensure that the two coils are decoupled. In addition, the adjacent secondary or relay coils are wound in the same direction to effectively enhance the coupling capability. By integrating the relay and the secondary coils, simultaneous power supply to multiple loads in the coaxial direction is achieved. However, all the receiving coils are required to be absolutely axisymmetric positioned to realize the consistence and the uniform distribution of the power received. Moreover, a planar PCB coil has been proposed for unmanned aerial vehicles by offering power to multiple loads radially, without the need for a battery and reduced weight [12]. Unfortunately, the power transfer capability is limited due to the limited operating frequency. Furthermore, a coupling structure for wide-range power transfer has been proposed for multiple loads that are located anywhere on the surface of the primary side [1]. However, load power distribution and regulation are not available while charging.

The design of the coupling structure in an MIMO IPT converter mainly includes cross-coupling and multi-group one-to-one coupling. Specifically, the inter-coil coupling inductance is considered in the cross-coupling structure, while the multi-group one-to-one coupling structure preserves the transfer properties of the original SISO coupling structure, thus simplifying the control procedure. To address the issue of power distribution, Nguyen et al. [13] have proposed an MIMO coupling structure with a set of relay coils. By changing the relative positions of the relay coils and the angles between the transmitting and receiving coils, the output power at the corresponding load side can be regulated. Since the relay coils must be placed between the transmitting and the receiving coils, it is difficult to adjust the swing angles precisely, and the distance among adjacent receiving coils should be fixed to ensure uniform power distribution. Recently, a multi-load IPT system applied has been proposed for charging electric vehicles [14]. The on/off of the power supply coils are controlled by detecting the parameter of mutual inductance, thereby selecting the appropriate power supplies for the various loads. However, specific design conditions of identical size and perfect alignment for transmitting and receiving coils are desirable for ensuring effective power transfer. In the design of array coupling structures of MIMO IPT converters, appropriate Litz windings with certain ferrite cores and PCB boards are chosen for specific applications. For example, a single-layer winding array and receiver coil structure with cylindrical ferrite core has been proposed [15], using Litz wires uniformly wound on a columnar ferrite. The structure is suitable for wireless charging with a user-friendly free-positioning feature for low-power applications. However, the consistency of the winding parameters cannot be guaranteed. In order to ensure consistent array parameters, a PCB array coil for small electronic devices has also been proposed [10]. The transmitting coil is composed of a double layer array, and the receiving coil adopts the same size of PCB array as the transmitting side. The design simplifies the charging of objects in blind spots and the installation in low-power applications. As load or power detection is not available in this IPT structure, all array coils are required to be powered simultaneously during the operation. Although a considerable amount of work has been reported on the use of various coupling structures for multi-load IPT systems, a unified design principle that can be systematically applied for designing multi-load converters is still missing [16,17].

In this paper, a unified design principle for standardized IPT systems is presented, providing appropriate control strategies that can be applied to a variety of coupling structures including SISO, SIMO, MISO and MIMO structures. Specifically, we start with the basic transfer features of a series–series (S/S) compensated SISO IPT system, including output power, transfer efficiency, operating conditions for achieving constant output, and so on [18]. Then, based on a set of common requirements of input and output terminals in various operating scenarios, SIMO, MISO and MIMO structures will be extended and

discussed. Finally, a unified set of design procedures for these structures will be developed, according to the operating conditions of the loads. Furthermore, simplified control strategies will be presented.

This paper is organized as follows. Section 2 provides the transfer characteristics of S/S compensated IPT converters with various coupling structures based on an equivalent circuit model. Section 3.1 presents power distribution strategies and IPT structure selection methods that address the various operating requirements of the output such as load type, power level and constant output conditions. A new control strategy for regulation of the output power is also discussed. In Section 3.2, a unified design flow of IPT systems that is applicable to various load types is given. Experimental verification is provided in Section 4. Section 5 concludes the paper.

2. Coupling Structures

2.1. Single-Input Double-Output Structure

Due to the existence of multi-load conditions in the system, the mutual inductance varies nonlinearly with the relative position when the coils at the receiving end are in the same plane. In the theoretical calculation stage, the calculation can be done in two categories. (1) The system has cross-coupling, i.e., the mutual inductance $M_{S1S2} \neq 0$. (2) The system does not have cross-coupling, i.e. the mutual inductance $M_{S1S2} = 0$. In practice, in order to avoid the cross-coupling problem between the transmitting coils, the transmitting coils are required to be reasonably designed, and the hardware decoupling can be realized by coil overlapping or placing away from each other. Moreover, to ensure a stable power transfer process, position and size identification strategies and several array coil switches are usually added in the source-level control system, making control more difficult. In order to ensure the consistency of coupling performance, the equal-size receiving coil structure is adopted in this paper, while the structure with a large transmitting coil is designed to achieve that the mutual inductance of the transmitting and receiving coils remains constant within a certain power supply range of the receiving coil.

Shown in Figure 1 is the equivalent circuit of a single-input double-output (SIDO) IPT converter using series–series (S/S) compensation. To facilitate the analysis, we assume that the converter is terminated by an ideal sine AC voltage source V_{in} at the input side and two equivalent loads R_{L1} and R_{L2} at the output side. The transformer consists of a primary coil with the self-inductance L_P and two secondary coils with self-inductances L_{S1} and L_{S2}. Each inductor is connected with a series compensated capacitor. From Kirchhoff's voltage law (KVL), the state equation of the SIDO circuit is

$$
\begin{bmatrix} \dot{V}_{\text{in}} \\ 0 \\ 0 \end{bmatrix} = \begin{bmatrix} Z_P & -j\omega M_{PS1} & -j\omega M_{PS2} \\ -j\omega M_{PS1} & Z_{S1} & j\omega M_{S1S2} \\ -j\omega M_{PS2} & j\omega M_{S1S2} & Z_{S2} \end{bmatrix} \begin{bmatrix} \dot{I}_P \\ \dot{I}_{S1} \\ \dot{I}_{S2} \end{bmatrix} \tag{1}
$$

where M_{PSi} (i = 1, 2) denotes the mutual inductance between the primary coil and the i-th secondary coil, and $M_{PSi} = k\sqrt{L_P L_{Si}}$; k represents the coupling coefficient; M_{S1S2} denotes the mutual inductance between the two secondary coils; ω denotes the operating frequency; I_P, Z_P, I_{Si} and Z_{Si} are the current and total impedances at the primary and the i-th secondary side, respectively.

Using the resonance condition of $\omega = 1/\sqrt{L_p C_p} = 1/\sqrt{L_s C_s}$ and Equation (1), the current I_{Si} flowing through the i-th secondary side can be obtained as

$$
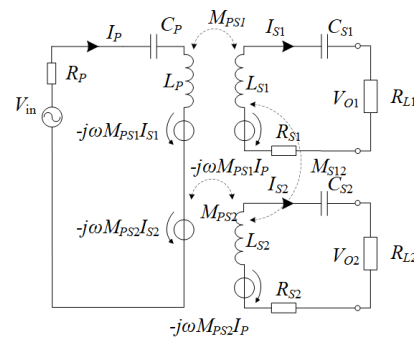I_{Si} = \frac{j\omega M I_P}{R_L + R_{si}} \tag{2}
$$

Figure 1. Equivalent circuit of a single-input double-output IPT circuit.

Based on the expression above, the output voltage V_{oi} of the i-th secondary side can be calculated as

$$V_{oi} = R_L I_{Si} = \frac{j\omega M V_{in} R_L}{(R_L + R_{si})R_p + \omega^2 M^2} \tag{3}$$

Assuming that both the secondary coils are placed in the same plane, the two coils are thus radially coupled. When the two coils are orthogonally positioned or are separated by a certain distance, the coupling coefficient k between the coils will be less than 0.01, i.e., $M_{S1S2} \approx 0$. Then, the equivalent reflected impedance Z_r of the SIDO system can be expressed as

$$Z_r = \frac{\omega^2 M_{PS1}^2}{Z_{S1}} + \frac{\omega^2 M_{PS2}^2}{Z_{S2}} \tag{4}$$

Since there exist several LC-resonant networks in the SIDO system, we define the self-resonance frequency as $\omega_P = 1/\sqrt{L_P C_P}$, $\omega_{Si} = 1/\sqrt{L_{Si} C_{Si}}$. Putting ω_P and ω_{Si} in (4), the real and imaginary parts of the reflected impedance Z_{ri} can be expressed separately as

$$\begin{cases} \Re(Z_{ri}) = \dfrac{\omega L_P k_{PSi}{}^2 Q_{Oi}}{1 + Q_{Oi}{}^2(1 - \xi_{Si}{}^2)^2} \\[3mm] \Im(Z_{ri}) = -\dfrac{\omega L_P k_{PSi}^2 Q_{Oi}^2(1 - \xi_{Si}{}^2)}{1 + Q_{Oi}^2\left(1 - \xi_{Si}{}^2\right)^2} \end{cases} \tag{5}$$

where $\xi_{Si} = \omega_{Si}/\omega$, $\xi_P = \omega_P/\omega$; Q denotes the quality factor of the component; $Q_{Li} = \omega L_{Si}/R_{Li}$; and $Q_{Oi} = \omega L_{Si}/(R_{Si} + R_{Li})$, $i = 1, 2$.

The whole system's efficiency can be divided into two parts: the primary-side and secondary-side efficiency. Using the impedance expressions, the transfer efficiency of the primary side can be obtained as

$$\eta_P = \frac{\Re(Z_{r1}) + \Re(Z_{r2})}{\Re(Z_{r1}) + \Re(Z_{r2}) + R_P}. \tag{6}$$

where parameter Z_{r1} and Z_{r2} are reflected impedances produced by secondary coils, and $\Re(Z_{ri})$ consists of ESR R_{si} and load resistance R_L.

The secondary-side power consists of output power and power consumed by the secondary-side topology. Thus, the secondary-side efficiency can be calculated by the ratio of output power to the total secondary-side power as

$$\eta_S = \frac{I_{S1}^2 R_{L1} + I_{S2}^2 R_{L2}}{I_{S1}^2 (R_{S1} + R_{L1}) + I_{S2}^2 (R_{S2} + R_{L2})} I_{S2}^2. \tag{7}$$

To facilitate the analysis, the two consistent coils are adopted at the secondary side. Then, the secondary-side efficiency can be simplified as

$$\eta_S = \eta_{S1}\eta_{S2} = \frac{(Q_{L1} + Q_{L2})}{(Q_{O1} + Q_{O2})} \frac{Q_{O1}Q_{O2}}{Q_{L1}Q_{L2}} \tag{8}$$

Substituting (5) into (6) and (8), the transfer efficiency η of the whole SIDO system is given by

$$\eta = \eta_P\eta_S = \frac{(Q_{L1} + Q_{L2})}{(Q_{O1} + Q_{O2})} \frac{Q_{O1}Q_{O2}}{Q_{L1}Q_{L2}} \left(\frac{\sum_{i=1}^{2} A_{Si}}{1 + \sum_{i=1}^{2} A_{Si}} \right) \tag{9}$$

where $A_{Si} = \dfrac{k_{PSi}^2 Q_P Q_{Oi}}{1 + Q_{Oi}^2 (1 - \xi_{Si}^2)^2}.$

When operating at the resonance frequency, i.e., $\xi_P = \xi_{Si} = 1$, the transfer efficiency can be simplified as

$$\eta = \frac{Q_P Q_{O1} Q_{O2} (Q_{L1} + Q_{L2})(Q_{O1} + Q_{O2})^{-1} Q_{L1}^{-1} Q_{L2}^{-1}}{1 + \left(k_{PS1}^2 Q_{O1} + k_{PS2}^2 Q_{O2} \right)^{-1}} \tag{10}$$

Combining (1), (5) and (10), the output power of the SIDO IPT system operating at the resonance frequency is given by

$$\begin{aligned} P_o &= \frac{V_{in}^2 \eta}{\sqrt{\left(R_P + \sum_{i=1}^{2} \Re(Z_r) \right)^2 + \Im(Z_r)^2}} \\ &= \frac{V_{in}^2 \frac{Q_{O1}Q_{O2}(Q_{L1}+Q_{L2})}{Q_{L1}Q_{L2}(Q_{O1}+Q_{O2})} \sum_{i=1}^{2} k_{PSi}^2 Q_P Q_{Oi}}{R_P \left(1 + \sum_{i=1}^{2} k_{PSi}^2 Q_P Q_{Oi} \right)^2} \end{aligned} \tag{11}$$

2.2. Double-Input Double-Output Structure

The transfer characteristics of a double-input double-output (DIDO) IPT converter can be extended from the above analysis. As shown in Figure 2, the two primary coils (equivalent to inductors L_{P1} and L_{P1}) of the DIDO converter are terminated by two independent sine AC voltage sources at the input side. The mutual inductance M_{P1P2} can be neglected when the two primary coils are orthogonally positioned or are separated by a certain distance. Thus, the transfer efficiency of the DIDO system is given by

$$\begin{cases} \eta = \prod_{j=1}^{2} \prod_{i=1}^{2} \eta_{Pj}\eta_{Si} \\ \eta_{Pj} = \dfrac{\sum_{i=1}^{2} \Re(Z_{rji})}{\sum_{i=1}^{2} \Re(Z_{rji}) + R_{Pj}} \\ \eta_{Si} = \dfrac{Q_{Oi}}{Q_{Li}} \end{cases} \tag{12}$$

The real and imaginary parts of the reflected impedance Z_{rji} of the *i*-th secondary side to the *j*-th primary side in (12) are

$$
\begin{cases}
\Re(Z_{rji}) = \dfrac{\omega L_{Pj} k_{ji}{}^2 Q_{Oi}}{1 + Q_{Oi}{}^2 (1 - \xi_{Si}{}^2)^2} = R_{Pj} A_{ji} \\[4mm]
\Im(Z_{rji}) = -\dfrac{\omega L_{Pj} k_{ji}{}^2 Q_{Oi}{}^2 (1 - \xi_{Si}{}^2)^2}{1 + Q_{Oi}{}^2 (1 - \xi_{Si}{}^2)^2} = -R_{Pj} B_{ji}
\end{cases}
\tag{13}
$$

where

$$
\begin{aligned}
A_{ji} &= \frac{k_{ji}{}^2 Q_{Pj} Q_{Oi}}{1 + Q_{Oi}{}^2 (1 - \xi_{Si}{}^2)^2}, \\[3mm]
B_{ji} &= \frac{k_{ji}{}^2 Q_{Pj} Q_{Oi}{}^2 (1 - \xi_{Si}{}^2)^2}{1 + Q_{Oi}{}^2 (1 - \xi_{Si}{}^2)^2}
\end{aligned}
$$

for $i, j = 1, 2$. Then, substituting (13) into (12) gives a simplified representation of efficiency, which leads to an expression for output power P_o of the DIDO IPT system as

$$
\begin{aligned}
P_o &= P_{\text{in}} \cdot \eta \\[2mm]
&= \prod_{j=1}^{2} \prod_{t=1}^{2} \frac{Q_{Ot}}{Q_{Lt}} \frac{\sum_{i=1}^{2} A_{ji}}{1 + \sum_{i=1}^{2} A_{ji}} \\[2mm]
&\quad \times \sum_{j=1}^{2} \frac{V_{\text{in}}{}^2}{R_{Pj} \sqrt{\left(1 + \sum_{i=1}^{2} A_{ji}\right)^2 + \sum_{i=1}^{2} B_{ji}{}^2}}
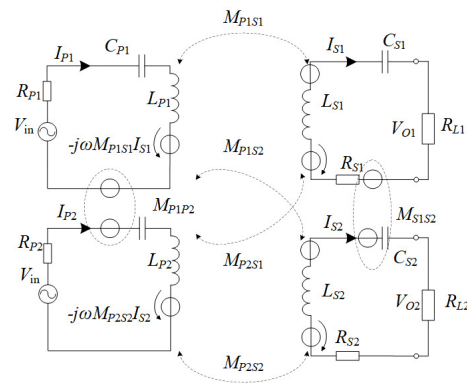\end{aligned}
\tag{14}
$$

Figure 2. Equivalent model of a double-input double-output IPT circuit.

2.3. General Multi-Input Multi-Output Structure

Based on the above analysis, a logical extension from the DIDO IPT converter to a multi-input multi-output (MIMO) IPT converter is possible, as shown in Figure 3, where *m* and *n* represent the number of primary and secondary coils, respectively. The corresponding transfer efficiency and output power can be readily obtained as follows:

$$
\eta = \prod_{j=1}^{m} \prod_{t=1}^{n} \frac{Q_{Ot}}{Q_{Lt}} \frac{\sum\limits_{i=1}^{n} A_{ji}}{1 + \sum\limits_{i=1}^{n} A_{ji}}
\tag{15}
$$

$$
\begin{aligned}
P_{\mathrm{o}} &= P_{\mathrm{in}} \cdot \eta \\
&= \prod_{j=1}^{m}\prod_{t=1}^{n} \frac{Q_{Ot}}{Q_{Lt}} \cdot \frac{\sum_{i=1}^{n} A_{ji}}{1 + \sum_{i=1}^{n} A_{ji}} \\
&\quad \times \sum_{j=1}^{m} \frac{V_{\mathrm{in}}{}^{2}}{R_{Pj}\sqrt{\left(1 + \sum_{i=1}^{n} A_{ji}\right)^{2} + \sum_{i=1}^{n} B_{ji}{}^{2}}}
\end{aligned}
\tag{16}
$$

where $Q_{Ot} = \omega L_{St}/(R_{St} + R_{Lt})$ and $Q_{Lt} = \omega L_{St}/R_{Lt}$, for $t = 1, \ldots, n$. Thus, we can obtain the transfer characteristics of any S/S compensated MIMO IPT converter under various operating conditions using the calculation results above. Here, with the requirement of load-independent output, the simple constant current (CC) output conditions are adopted. Both primary and secondary sides of the converter operate at the self-resonance frequency, i.e., $\omega_P = \omega_S = \omega$ and $\xi_P = \xi_S = 1$. Substituting these operating conditions into (13), it can be readily obtained that the factor $B_{ji} = 0$, and the simplified impedance Z_{rji} is given by

$$
Z_{rji} = k_{ji}{}^{2} R_{Pj} Q_{Pj} Q_{Oi}.
\tag{17}
$$

Then, the total transfer efficiency of an MIMO IPT converter with S/S compensation can be further simplified as

$$
\eta = \prod_{j=1}^{m}\prod_{t=1}^{n} \frac{Q_{Ot}}{Q_{Lt}} \frac{\sum_{i=1}^{n} k_{ji}^{2} Q_{Oi}}{1 + \sum_{i=1}^{n} k_{ji}^{2} Q_{Oi}}
\tag{18}
$$

Similarly, the total output power of the MIMO IPT converter is simplified as

$$
P_{\mathrm{o}} = \prod_{j=1}^{m}\prod_{t=1}^{n} \frac{Q_{Ot}}{Q_{Lt}} \frac{\sum_{i=1}^{n} k_{ji}{}^{2} Q_{Oi}}{1 + \sum_{i=1}^{n} k_{ji}{}^{2} Q_{Oi}} \sum_{j=1}^{m} \frac{V_{\mathrm{in}}{}^{2}}{R_{Pj}(1 + \sum_{i=1}^{n} k_{ji}{}^{2} Q_{Oi})}
\tag{19}
$$

Assuming that the system parameters of each input or output branch are consistent with the MIMO IPT converter, the total output power given in (19) becomes

$$
P_{\mathrm{o}} = \frac{m U_{i}^{2} Q_{O}{}^{n} (n k^{2} Q_{P} Q_{O})^{m}}{R_{P} Q_{L}{}^{n} (1 + n k^{2} Q_{P} Q_{O})^{m+1}}
\tag{20}
$$

In order to achieve maximum power output, we differentiate (20) with respect to R_L, giving the optimal load value as

$$
\begin{aligned}
R_{L,P_m} =\ & \frac{1}{2m}\Bigg[R_S(n-m) + \frac{\omega^{2} M^{2} n}{R_P} \\
& + \frac{1}{R_P}\Bigg(\Big(R_S R_P(n-m) - \omega^{2} M^{2} n \Big)^{2} \\
& + 4mn R_S(\omega^{2} M^{2} n + R_S R_P) \Bigg)^{\frac{1}{2}} \Bigg]
\end{aligned}
\tag{21}
$$

Thus, by transitioning from SIDO IPT circuits to DIDO IPT circuits, and finally extending to a generic MIMO IPT circuit, we can obtain theoretical results for the transfer features of any MIMO IPT circuit with S/S compensation based on the above formulas. Accordingly, the optimal operating point for maximum power output or maximum efficiency transfer can be calculated. In this paper, the normal operation of each load is mainly concerned. Then, the priority of maximum power output is considered as higher than maximum efficiency transfer. Therefore, the unified design will be centered on power distribution and regulation. The above formulas will also be used later in our proposed unified design procedure.
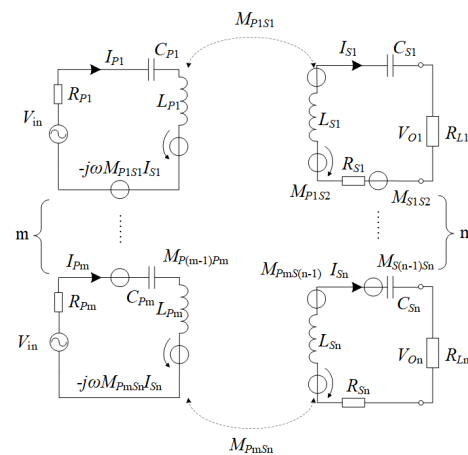
Figure 3. Equivalent model of a multi-input multi-output IPT circuit.

2.4. Illustrations by Simulations

In order to reveal the load characteristics of multi-output IPT systems, we present simulations based on the equivalent model shown in Figure 1. The parameter values listed in Table 1 are used. From Figure 4a, it can be readily observed that with a certain value of R_{L1}, the power delivered to R_{L1} increases as R_{L2} increases, and the growth gradually slows down. Similar results can be observed from Figure 4b. In addition, the maximum power transfer points to R_{L1} and R_{L2} can be identified. Likewise, Figure 5 illustrates the trend of the transfer efficiency as the values of R_{L1} and R_{L2} increase. With one load fixed, the optimal efficiency point of the other load can be readily identified.

In short, from the foregoing illustration, the output power of each load in a multi-load IPT system is affected by the change of resistance in either load of the system. Thus, when the number of output terminals changes, regulation of the output power or equivalent load value is necessary to achieve maximum power transfer.
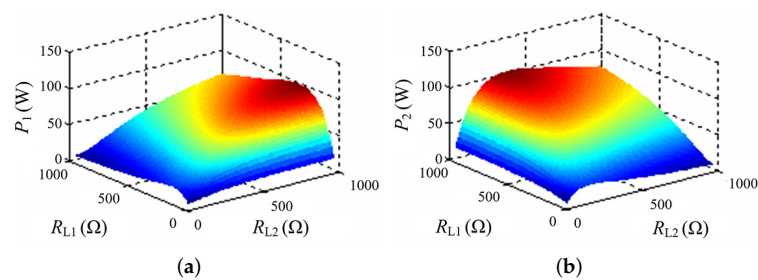

(a)

(b)

Figure 4. (**a**) Simulated output power on R_{L1} versus value of R_{L2}; and (**b**) output power on R_{L2} versus value of R_{L1}.
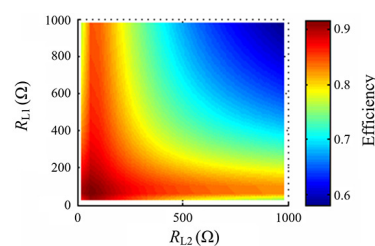

Figure 5. Simulated transfer efficiency versus load.

Table 1. Simulation Parameters of Single-Input Double-Output IPT Circuits.

Parameter	Value
Primary inductor L_P	230 μH
Secondary inductor L_{S1}, L_{S2}	100 μH
Coupling coefficient k_{PS1}, k_{PS2}	0.19
Operating frequency f	100 kHz
ESR R_P	0.4 Ω
ESR R_{S1}, R_{S2}	0.2 Ω
Input voltage V_{in} (rms)	50 V

3. Control and Design Principles

3.1. Load Control

As mentioned in Section 2, the primary and secondary sides of the MIMO IPT system with S/S compensation operate at the same resonance frequency ω. In this case, A_{ji} and B_{ji} in the Z_{ji} expression (13) are

$$\begin{cases} A_{ji} = k_{ji}{}^2 Q_{Oi} \\ B_{ji} = 0, \end{cases} \tag{22}$$

implying that the input impedance Z_{ji} is purely resistive; i.e., zero phase angle (ZPA) input is achieved. Since the output current of the system is independent of the load, using the standard transfer ratio expression of S/S compensated IPT circuit with LIC output [19], we obtain the output current I_{oi} of the i-th secondary side as

$$I_{oi} = \sum_{j=1}^{m} \frac{V_{in}}{\omega M_{PjSi}} \tag{23}$$

As discussed in Section 2.4, in order to fulfill the power required for normal operation of the load and the maximum power output condition when the number of input and output terminals varies, it is necessary to regulate the load resistance R_L without changing the coupling parameters of the IPT system.

In the following, a control strategy is presented to conveniently set the load resistance to the desired value. Assume that the equivalent resistance of each load is the same, and the coupling distance between each primary coil and the i-th secondary coil does not vary a lot. Then, each output terminal of the IPT system is expected to deliver the same current value.

Shown in Figure 6a is the equivalent circuit of a tunable resistor R_L, consisting of an initial resistor R_{L0} and a variable resistor R_{var}, i.e., $R_L = R_{L0} + R_{var}$. By adjusting the duty cycle D of the anti-parallel MOSFETs connected in parallel with resistor R_{var}, the value of R_L can be controlled. Here, the duty cycle D can be tuned from 0 to 1. Parameters R_{var} and R_{L0} are both pure resistance with fixed value, and R_{L0} can be set to the same value as R_{var} to achieve a wide tunable range of the duty cycle. Thus, the number of secondary coils depends on parameters D and R_{var}. The corresponding waveforms of the initial current i_0, the PWM wave, the current i_{var} flowing through R_{var}, and the output power delivered to R_{var} are illustrated in Figure 6b. The conduction angle can be adjusted by controlling duty cycle D, thus regulating the equivalent output power P_{var}. Specifically, the alignment position of the PWM signal is πD in a current cycle. By detecting the zero-crossing current and delaying the angle by $(\pi/2 - \pi D/2)$, precise control of the load resistance can be achieved. Thus, the equivalent load value R_{var} with initial resistance of R_{L0} can be expressed in terms of duty cycle D as

$$\frac{R_{var}}{R_{L0}} = \frac{I_0^2}{I_{var}^2} = 1 - D - \frac{1}{\pi}\sin(\pi D). \tag{24}$$

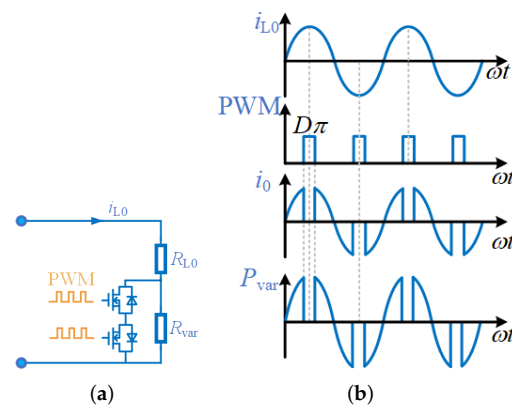The relationship between the ratio of R_{var} to R_{L0} and the duty cycle D is illustrated in Figure 7.

Figure 6. (**a**) Equivalent circuit and (**b**) corresponding theoretical waveforms of a tunable resistor R_L.

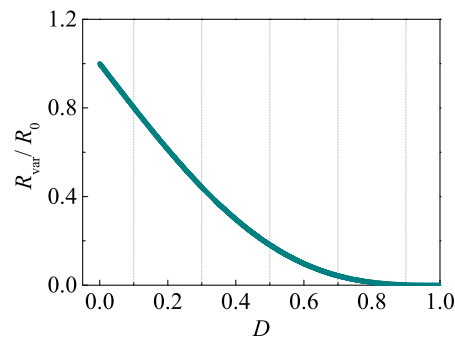**Figure 7.** Ratio R_{var}/R_0 versus duty cycle D.

3.2. Design Principle

In this section, a design process for MIMO IPT systems with optimal power output is presented. Let P_E represent the total rated power of the loads and P_o denote the output power capacity of the system. The design procedure starts with a single-input structure, and the series of steps are:

1. Obtain the load information, e.g., number of outputs n, rated output P_E, and operating conditions.
2. Determine if a single-output or multi-output structure is required.
3. Obtain theoretical results of output power P_o and the equivalent reflected impedance Z_r using the procedure given in Section 2.
4. If P_o exceeds P_E, retain the single-input structure and calculate the desired optimal load value for each load using Equation (21) in Section 2, or calculate the value of load under normal operating conditions using Ohm's Law. Otherwise, choose the multi-input structure and go back to Step 2.
5. Apply the load control to regulate the load value(s) to the optimal point(s) based on the control strategy presented in Section 3.1.

As the equivalent load of each output is set to the optimal value, maximum power output can be achieved.

4. Experimental Validation

In order to verify the analysis presented above, a laboratory prototype based on the SIDO IPT system is constructed, using the configuration of Figure 8, a photo of which is shown in Figure 9. To simplify the design of the load side, the same structure of the secondary coil is used with a different value of load resistance. Moreover, to estimate the mutual inductance between the two secondary coils, a large primary coil is adopted in this experiment, and the two secondary coils are symmetrically arranged with respect to the

primary coil (i.e., diagonally positioned), as illustrated in Figure 10, thus ensuring the same mutual inductance between the receiver and the transmitter, i.e., $M_{PS1} = M_{PS2}$.
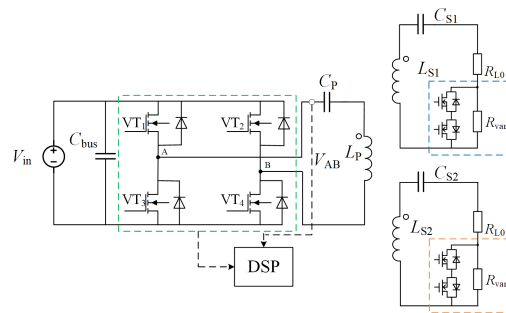

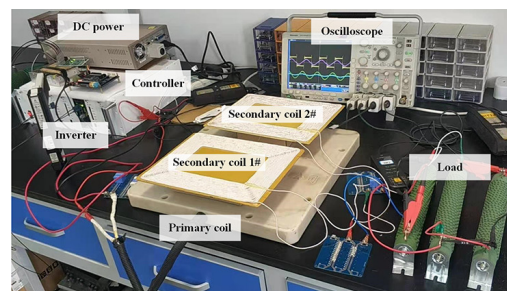**Figure 8.** Configuration of experimental single-input double-output IPT system.
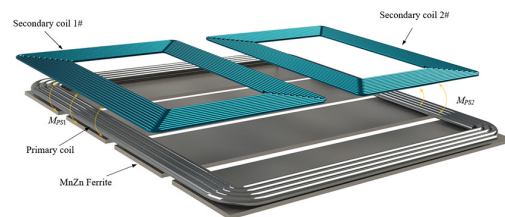

Figure 9. Experimental setup.

Figure 10. Layout of coupling structure used in experimental single-input double-output IPT system.

As shown in Figure 8, the designed configuration consists of a DC power supply, a high-frequency inverter, a transformer composed by a primary coil (transmitter) and two secondary coils (receiver), compensation circuits and the corresponding controller. The bus DC voltage source is supplied to the H-bridge inverter made up of SiC power components (C2M0080120), which have low conduction and switching losses. Current detection and protection circuits for the inverter are included to ensure the stability of the switching devices. The threshold of the detection and protection current is set to 7 A. Parameter V_{AB} represents the output voltage of the H-bridge inverter. For the compensation components, NPO ceramic capacitors are utilized as the compensation capacitors for both primary and secondary sides to minimize the effect of temperature on the capacitances, thus ensuring the stability of resonance parameters. The values of the components used in the experiment are shown in Table 2.

Figure 11 illustrates the coupling performance of the two receiving coils. It can be observed that as the gap D between the two planar coils changes, the mutual coupling coefficient M_{S1S2} also changes. When the gap increases to about one-sixth the coil width, the coupling performance reaches an inflection point, and its value is much lower than the value of M_{PS1} or M_{PS2} between the transmitter and receiver. In this case, the influence between the receiving coils can be approximately ignored. That is, when the gap between the receiving coils becomes greater than one-sixth the coil width, the mutual inductance between the coils can be approximately equivalent to zero.

Table 2. Parameters of Experimental Single-Input Double-Output IPT Circuit.

Parameter	Value
Primary inductor L_P	228.45 μH
Secondary inductor L_{S1}	99.58 μH
Secondary inductor L_{S2}	98.23 μH
Primary capacitor C_P	11.2 nF
Secondary capacitor C_{S1}	25.8 nF
Secondary capacitor C_{S2}	26.2 nF
Transformer size (primary)	475×475 mm^2
Transformer size (secondary)	327×245 mm^2
Type of Litz wire	0.1×900
No. of primary turns	18
No. of secondary turns	24
Ferrite size	$100 \times 100 \times 10$ mm
Ferrite type	PC95
Relative permeability	3300
Wire diameter	5 mm
Coupling coefficient k_{PS1}, k_{PS2}	0.19
Operating frequency f	100 kHz
Input voltage V_{in}	50 V

To compare the performance of IPT systems with various output terminals at various load resistance, only one output terminal of the system in Figure 8 is adopted first, which changes the SIDO system to an SISO system with the same parameters. Then, the SIDO system is evaluated with the same load value as in the SISO system. Figure 12 shows the measured waveforms of the SISO IPT configuration when the load resistance is regulated to the optimal point of 10 Ω with the maximum output power of 31.2 W.
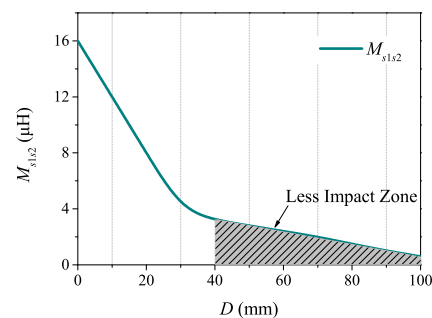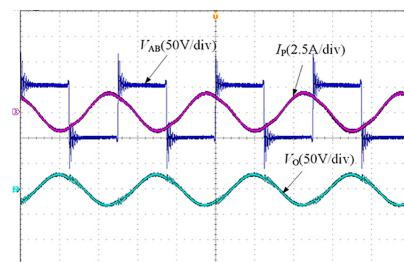

Figure 11. Coupling between adjacent secondary coils.

Figure 12. Measured waveforms of single-input single-output IPT system with $R_L = 10$ Ω.

Figure 13 shows the measured waveforms of the SIDO IPT configuration when the two secondary coils are connected to loads with the same equivalent resistance of 10 Ω. The measured waveforms indicate that the output power of each load is approximately

20.2 W, which is below the required power level of the load, and the load value is not the optimal point.
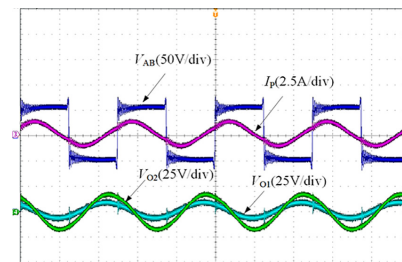

Figure 13. Measured waveforms of single-input double-output IPT system with $R_{L1} = R_{L2} = 10\ \Omega$.

Figure 14 shows the measured waveforms of the SIDO IPT configuration when the control is applied to regulate the resistance of load R_{L2} to the optimal point of 30.5 Ω while keeping R_{L1} unchanged. It can be observed that the output power of load R_{L2} increases to 33.7 W. Figure 15 shows the measured results of output power changes with the load value of the SISO configuration. Figure 16 shows the measured output power versus load value of SIMO configurations with and without load control. It can be observed from these two figures that when the load resistance is tuned from 50 to 70 Ω via load control, the output power of the SIDO system steps up from 58 W to 98 W, which nearly reaches the output power level of the SISO system. Both the measured and theoretical results reveal that by adjusting the load value, it is possible to achieve a variety of power output combinations for different loads as well as to better meet the output requirements of different load characteristics. Furthermore, by regulating the equivalent resistance of the load to the optimal point, maximum power output can be preserved despite variation in the output terminals.
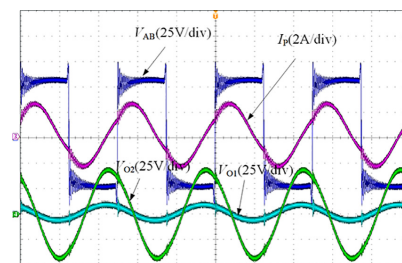

Figure 14. Measured waveforms of single-input double-output IPT system with $R_{L1} = 10\ \Omega$, $R_{L2} = 30.5\ \Omega$.
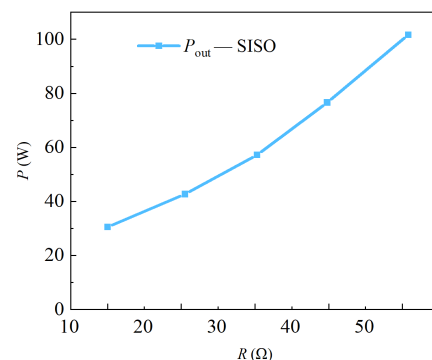

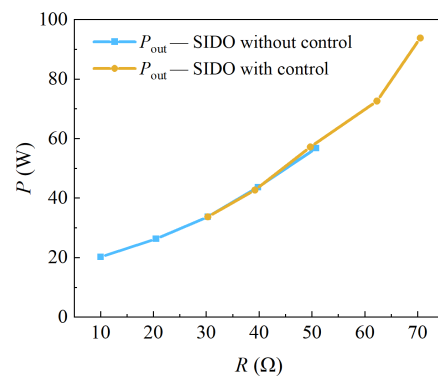**Figure 15.** Output power versus load of SISO configuration.

Figure 16. Output power versus load of SIDO configuration.

5. Conclusions

This paper attempts to provide general design guidelines for inductive power transfer (IPT) systems for multi-load applications. Transfer characteristics and the respective suitable applications of various coupling structures with series–series (S/S) compensations are discussed in detail via circuit analysis based on mutual-inductance models. A set of design procedures of IPT systems is proposed to meet various operating conditions, power requirements and the number of loads. Furthermore, phase-shift control strategies at the load side are presented to permit an optimal power output with various load impedance. A single-input double-output IPT configuration is constructed for experimental validation. The measured results explicate that after the load resistance is tuned to the optimal value via load control, the output power has increased by 66.8%.

Institutional Review Board Statement: Not applicable.

Informed Consent Statement: Not applicable.

Data Availability Statement: Not applicable.

Conflicts of Interest: The authors declare no conflict of interest.

References

1. Wang, Z.; Li, Y.; Sun, Y.; Tang, C.; Lv, X. Load Detection Model of Voltage-Fed Inductive Power Transfer System. *IEEE Trans. Power Electron.* **2013**, *28*, 5233–5243. [CrossRef]
2. Xia, C.; Liu, L.; Liu, Y.; Ma, Z. IPT system for tail-free household appliances in the smart home system. *IET Power Electron.* **2019**, *12*, 1002–1010. [CrossRef]
3. Covic, G.A.; Boys, J.T. Inductive power transfer. *Proc. IEEE* **2013**, *101*, 1276–1289. [CrossRef]
4. Budhia, M.; Boys, J.T.; Covic, G.A.; Huang, C. Development of a single-sided flux magnetic coupler for electric vehicle IPT charging systems. *IEEE Trans. Ind. Electron.* **2013**, *60*, 318–328. [CrossRef]
5. Zaheer, A.; Covic, G.A.; Kacprzak, D. A bipolar pad in a 10-kHz 300 W distributed IPT system for AGV applications. *IEEE Trans. Ind. Electron.* **2014**, *61*, 3288–3301. [CrossRef]
6. Zhang, Y.; Lu, T.; Zhao, Z.; He, F.; Chen, K.; Yuan, L. Employing Load Coils for Multiple Loads of Resonant Wireless Power Transfer. *IEEE Trans. Power Electron.* **2015**, *30*, 6174–6181. [CrossRef]
7. Sarnago, H.; Burdío, J.; Lucía, Ó. High-Performance and Cost-Effective ZCS Matrix Resonant Inverter for Total Active Surface Induction Heating Appliances. *IEEE Trans. Power Electron.* **2019**, *34*, 117–125. [CrossRef]
8. Wireless Power Consortium Website. Available online: http://www.wirelesspowerconsortium.com (accessed on 1 January 2022).

9. Zhong, W.; Liu, X.; Hui, S.Y. Analysis on a single-layer winding array structure for contactless battery charging systems with free-positioning and localized charging features. In Proceedings of the IEEE Energy Conversion Congress and Exposition (ECCE), Atlanta, GA, USA, 12–16 September 2010; pp. 658–665.

10. Meyer, P.; Germano, P.; Markovic, M.; Perriard, Y. Design of a contactless energy-transfer system for desktop peripherals. *IEEE Trans. Ind. Appl.* **2011**, *47*, 1643–1651. [CrossRef]

11. Cheng, C.; Zhou, Z.; Li, W.; Zhu, C.; Deng, Z.; Mi, C. A multi-load wireless power transfer system with series-parallel-series compensation. *IEEE Trans. Power Electron.* **2019**, *34*, 7126–7130. [CrossRef]

12. Arteaga, J.; Aldhaher, S.; Kelis, G.; Kwan, C.; Yates, D.; Mitcheson, P. Dynamic capabilities of multi-MHz inductive power transfer systems demonstrated with batteryless drones. *IEEE Trans. Power Electron.* **2018**, *34*, 5093–5104. [CrossRef]

13. Nguyen, M.; Chou, Y.; Plesa, D.; Rao, S.; Chiao, J. Multiple-inputs and multiple-outputs wireless power combining and delivering systems. *IEEE Trans. Power Electron.* **2015**, *30*, 6254–6263. [CrossRef]

14. Vu, V.; Phan, V.; Dahidah, M.; Pickert, V. Multiple output inductive charger for electric vehicles. *IEEE Trans. Power Electron.* **2018**, *34*, 7350–7368. [CrossRef]

15. Zhong, W.; Liu, X.; Hui, S.Y.R. A novel single-layer winding array and receiver coil structure for contactless battery charging systems with free-positioning and localized charging features. *IEEE Trans. Power Electron.* **2010**, *58*, 4136–4144. [CrossRef]

16. Luo, Y.; Yang, Y.; Wen, X.; Cheng, M. Enhancing the Robustness of the Wireless Power Transfer System to Uncertain Parameter Variations Using an Interval-Based Uncertain Optimization Method. *Energies* **2018**, *11*, 2032. [CrossRef]

17. Zhang, Z.; Tong, R.; Liang, Z.; Liu, C.; Wang, J. Analysis and Control of Optimal Power Distribution for Multi-Objective Wireless Charging Systems. *Energies* **2018**, *11*, 1726. [CrossRef]

18. Qu, X.; Jing, Y.; Han, H.; Wong, S.C.; Tse, C.K. Higher order compensation for inductive-power-transfer converters with constant voltage or constant-current output combating transformer parameter constraints. *IEEE Trans. Power Electron.* **2017**, *32*, 394–405. [CrossRef]

19. Liu, Y.C.; Zhang, J.; Tse, C.K.; Zhu, C.; Wong, S.C. General Pathways to Higher Order Compensation Circuits for IPT Converters Via Sensitivity Analysis. *IEEE Trans. Power Electron.* **2021**, *36*, 9897–9906. [CrossRef]